Meteoritics & Planetary Science 40, Nr 3, 377–396 (2005)
Abstract available online at http://meteoritics.org

Melt inclusions in augite of the Nakhla martian meteorite: Evidence for basaltic parental melt

Karen Renée STOCKSTILL,[1*] Harry Y. MCSWEEN, Jr.,[1] and Robert J. BODNAR[2]

[1]Department of Earth and Planetary Sciences and Planetary Geosciences Institute, University of Tennessee, Knoxville, Tennessee 37996–1410, USA
[2]Department of Geological Sciences, Virginia Polytechnic Institute and State University, Blacksburg, Virginia 24061–0420, USA
*Corresponding author. E-mail: kstockst@utk.edu

(Received 09 June 2004; revision accepted 20 December 2004)

Abstract–Nakhla contains crystallized melt inclusions that were trapped in augite and olivine when these phases originally formed on Mars. Our study involved rehomogenization (slow-heating and fast-heating) experiments on multiphase melt inclusions in Nakhla augite. We studied melt inclusions trapped in augite because this phase re-equilibrated with the external melt to a lesser extent than olivine and results could be directly compared with previous Nakhla melt inclusion studies. Following heating and homogenization of encapsulated melt inclusions, single mineral grains were mounted and polished to expose inclusions. Major element chemistry was determined by electron microprobe. The most primitive melt inclusion analyzed in Nakhla NA03 is basaltic and closely matches previously reported nakhlite parent melt compositions. MELTS equilibrium and fractional crystallization models calculated for NA03 and previous Nakhla parent melt estimates at QFM and QFM-1 produced phase assemblages and compositions that can be compared to Nakhla. Of these models, equilibrium crystallization of NA03 at QFM-1 produced the best match to mineral phases and compositions in Nakhla. In all models, olivine and augite co-crystallize, consistent with the hypothesis that olivine is not xenocrystic but has undergone subsolidus re-equilibration. In addition, measured melt inclusion compositions plot along the MELTS-calculated liquid line of descent and may represent pockets of melt trapped at various stages during crystallization. We attempt to resolve discrepancies between previous estimates of the Nakhla parental melt composition and to reinterpret the results of a previous study of rehomogenized melt inclusions in Nakhla. Melt inclusions demonstrate that Nakhla is an igneous rock whose parent melt composition and crystallization history reflect planetary igneous processes.

INTRODUCTION

Melt inclusions are solidified pockets of melt (usually with diameters of a few hundred μm or less) trapped during crystal growth. They represent the liquids from which their host crystals grew (Anderson 1979; Danyushevsky et al. 2002a; Frezzotti 2001; Roedder 1979; Sobolev 1996), and inclusions encapsulated at different times can provide a record of evolving melt compositions. Melt inclusions may be used to determine major and trace element concentrations and abundances of volatiles (H_2O, CO_2, Cl, S, etc.) in the melt, as well as melt density (Lowenstern 1995; Newman et al. 1988; Sisson and Layne 1993; Wallace et al. 1999). They are particularly useful in reconstructing the parent melts of cumulate rocks.

Unhomogenized melt inclusions in the augite and olivine of nakhlite meteorites (thought to be martian igneous rocks, as reviewed by Treiman et al. [2000]) contain an assortment of daughter crystals, including the host phase that forms on the walls of the inclusion, that grew after the melt was trapped (Fig. 1). These are commonly referred to as multiphase or crystallized inclusions to distinguish them from glassy inclusions. Multiphase melt inclusions in augite range from <10 to 75 μm; however, inclusions over 20 μm are rare. Their shapes vary from negative crystal morphologies to rounded. Multiphase melt inclusions commonly occur in clusters, rather than individually, and are ubiquitous in most augite grains (Fig. 1a). The post-entrapment daughter mineral visible during petrographic examination of the inclusions is an Fe-Ti oxide (due to its reflectivity, this phase is visually distinct from the glass of the inclusion and the surrounding host mineral). In addition, augite precipitated on the inclusion

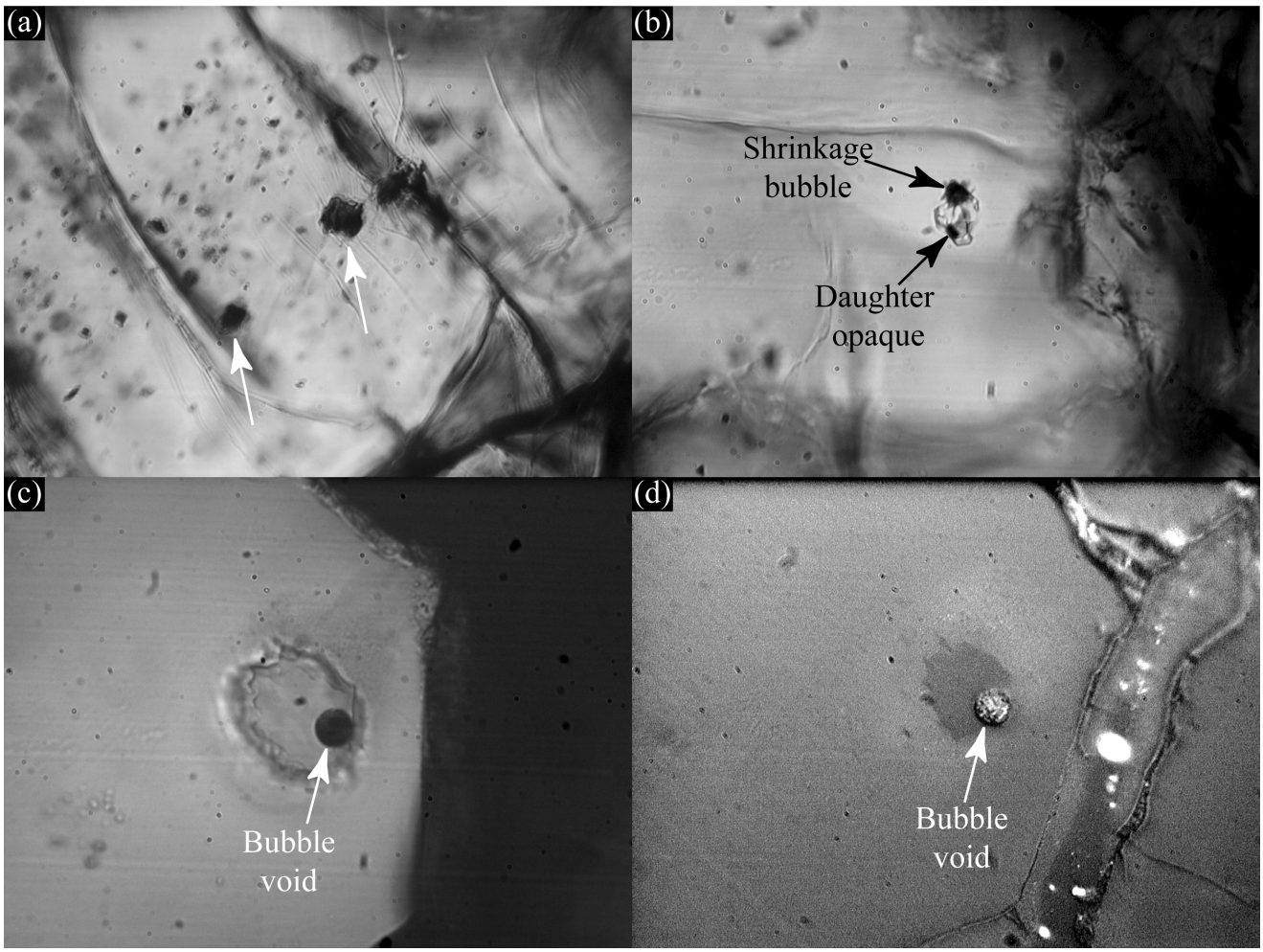

Fig. 1. a) Low magnification view (40×) of Nakhla augite containing several unhomogenized melt inclusions at variable depths within the crystal. The field of view is 4 mm. Fields of view for all other photomicrographs are 2 mm across. b) Transmitted light photomicrograph of an unhomogenized 10 μm melt inclusion in a Nakhla augite. A shrinkage bubble and daughter opaque phase are visible in this view. c) Transmitted light photomicrograph of a homogenized 20 μm melt inclusion in Nakhla that has been exposed at the surface following homogenization. d) Same melt inclusion in reflected light. In both views, the bubble void is visible. Notice that the full melt inclusion diameter has not been exposed at the surface.

walls following entrapment of the melt-material that is not visibly distinct via petrographic inspection. Bubble voids, either formed by shrinkage (due to volume change of glass during cooling) or representing volatiles exsolved from the melt during cooling, are also observable. The bubble voids represent only a few percent of the inclusion volume (Lowenstern 1995). To obtain a homogeneous glass for electron microprobe analysis, it is necessary to heat multiphase inclusions to redissolve the daughter phases. Once the melt inclusion is rehomogenized, the sample can be quenched to produce a glass, at which point it can be referred to as a melt inclusion.

Previous researchers have estimated the composition of nakhlite parental melts by a variety of techniques. Longhi and Pan (1988) calculated major element oxide concentrations in the melt using augite-liquid partition coefficients from experiments that produced Nakhla-like augites, constraining the melt to lie on or near the olivine-augite liquidus and using the composition of Nakhla augite cores to locate it along the liquidus. This composition plots within the basalt field on the total alkali-silica (TAS) diagram (Fig. 2a) and within the augite field on the olivine (projection)-orthopyroxene-wollastonite-plagioclase phase diagram (Fig. 2b). Harvey and McSween (1992a) analyzed glass and daughter minerals in multiphase melt inclusions in olivine grains of Nakhla and Governador Valadares and employed mass-balance calculations to estimate the original melt inclusion composition. Like Longhi and Pan (1988), they considered only compositions that fell on or near the augite-olivine phase boundary to be representative of the parent liquid. Their favored composition for Nakhla falls in the TAS basalt field (Fig. 2a) and within the augite field of the olivine projection (Fig. 2b). Treiman (1993) studied multiphase melt inclusions from Nakhla olivine as well, but used rastered or defocused-

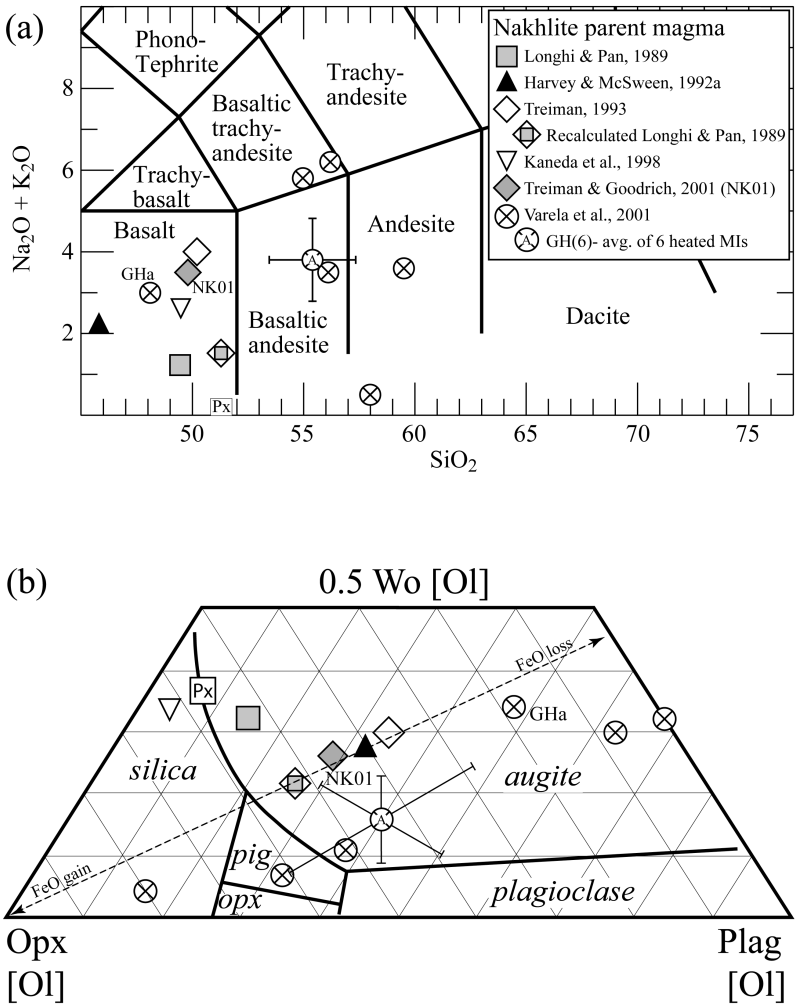

Fig. 2. Published estimates of SNC parental magma compositions and previously heated melt inclusion compositions plotted on a) the total alkali-silica (TAS) diagram and b) an orthopyroxene-wollastonite-plagioclase phase diagram projected from olivine (after Longhi 1991). Most previous estimates of SNC parental magma compositions plot within the basalt field on the TAS and within the augite field of the olivine projection. The host pyroxene phase for melt inclusions is represented by "Px" within a square. FeO loss and gain is represented by a double-arrow dashed line and is important when considering re-equilibration of olivine.

beam electron microprobe analyses to determine the bulk composition of the largest melt inclusions. A weighted average of these compositions was calculated, followed by olivine subtraction to account for host olivine analyzed by the rastered beam, and finally the addition of daughter olivine that plated out on the walls of the inclusion following entrapment. This composition was then adjusted to be in equilibrium with co-existing augite cores and thus to liquids co-saturated with augite and olivine. The final parental melt composition plots within the TAS basalt field (Fig. 2a) and within the augite field of the olivine projection (Fig. 2b). Treiman (1993) also recalculated the estimates of Longhi and Pan (1988) using a new average analysis of Nakhla core augite to produce a second composition, which plots within the TAS basalt field (Fig. 2a) with low total alkali content (1.5%) and plots within the augite field on the olivine projection (Fig. 2b). Kaneda et al. (1998) estimated the Nakhla parental melt composition from compositions used in their crystallization experiments. These experiments produced augites that exhibited the natural core compositions and the zoning patterns seen in Nakhla pyroxenes. The starting composition that produced the best match to Nakhla pyroxenes plots within the TAS basalt field near other estimates of nakhlite parental melts (Fig. 2a), but within the silica field on the olivine projection (Fig. 2b). Treiman and Goodrich (2001) revised the Nakhla parent magma composition of Treiman (1993), principally by adjusting its (Fe, Mg)O content. Their preferred composition, NK01, plots in the TAS basalt field near other estimates (Fig. 2a) and within the augite field on the phase diagram (Fig. 2b). NK01 is the most recent and probably most accepted value of the Nakhla parent melt composition.

The only previous study of homogenized melt inclusions in Nakhla was preformed by Varela et al. (2001). Their average composition of six heated melt inclusions in Nakhla augites (GH(6) in Figs. 2a and 2b) was not in equilibrium with the host augite nor with co-existing olivine and they questioned the accepted igneous origin of this meteorite. However, it is not clear that this average value can be representative of an actual trapped melt, as discussed below. Their study also showed heterogeneity in alkali contents among the melt inclusions. The experiments produced glasses with compositions ranging from basalt to andesite on the TAS diagram (Fig. 2a) and plotting across several fields on the olivine projection (Fig. 2b). Because of the lack of equilibrium and the variation in alkali contents, Varela et al. (2001) suggested that glass-bearing inclusions in Nakhla augite are most likely heterogeneously trapped liquids and solids formed through nebular (non-igneous) processes.

The estimates of nakhlite parental magma compositions described above show wide variation. Because these meteorites contain cumulus phases (McSween 1994), their bulk compositions do not necessarily represent melt compositions (Longhi and Pan 1988). As part of this study, we reproduced the slow-heating homogenization experiments of Varela et al. (2001) on melt inclusions in Nakhla augite. However, several workers (Danyushevsky et al. 2002a; Nielsen et al. 1998; Qin et al. 1992; Sobolev et al. 1990) have called attention to problems with host-inclusion mass exchange associated with slow heating rates, which will be discussed in detail below. Thus, we also performed fast-heating homogenization experiments on melt inclusions in Nakhla augite. The major objectives of this study were to use rehomogenized melt inclusions to 1) better constrain the parental melt compositions for Nakhla and 2) resolve the question of whether Nakhla is an igneous rock, as believed by most previous researchers, or a nebular conglomerate, as proposed in the melt inclusion study of Varela et al. (2001).

SAMPLE PREPARATION, EXPERIMENTAL AND ANALYTICAL METHODS

An unweathered, pea-sized sample of Nakhla was obtained from the British Museum for melt inclusion studies. Doubly-polished "thick" sections (75–100 μm thick) were produced and then removed from glass slides by soaking in an acetone bath for several hours. Mineral grains were separated under a binocular microscope and examined at high power. Augite grains containing inclusions of sufficient size (i.e., electron microprobe analysis requires melt inclusions ≥10 μm) were isolated for heating experiments. Melt inclusions in these grains were completely enclosed by the host phase.

Melt inclusions in Nakhla are found within both augite and olivine. We chose to focus on melt inclusions in augite. The open-system behavior of olivine-hosted melt inclusions with respect to Fe/Mg exchange is well established (e.g., Danyushevsky et al. 2002b; Gaetani and Watson 2000), and nakhlite olivine appears to have re-equilibrated with the external melt to a greater degree than the co-existing augite (e.g., Harvey and McSween 1992a; Longhi and Pan 1988). The augites have nearly homogeneous cores ($Wo_{38–41}En_{37–40}Fs_{22–23}$ and Fe/Mg = 0.55–0.62) and narrow rims that are zoned with increasing Fe/Mg ratios ($Wo_{33–41}En_{21–37}Fs_{26–44}$ and Fe/Mg = 0.70–1.97) (Friedman Lentz et al. 1999; McSween and Treiman 1998; Sautter et al. 2002). Augite cores appear to have preserved their original magmatic composition (Harvey and McSween 1992b), so augite-hosted inclusions should be closer to their original trapped composition. Furthermore, studying augite-hosted melt inclusions allows for direct comparison with the work of Varela et al. (2001).

The heating schedule is important during homogenization of multiphase melt inclusions. If the inclusions are heated too quickly, they may rupture or leak along fractures. If they are not held at high temperature for a sufficient length of time, the melt may not reach equilibrium with the host phase. Conversely, if the sample is heated too slowly or held at high temperature too long, the minerals may oxidize and become dark, precluding visual monitoring of the melting process, or excessive amounts of the host crystal may be incorporated into the melt. In addition, Sobolev et al. (1990) demonstrated that, with slow heating, mass exchange can occur between the inclusion and the host crystal. In particular, diffusion of hydrogen through the inclusion wall allows water to combine with FeO to produce titanomagnetite. Thus, even if the external atmosphere is reduced during heating, oxidation of the melt occurs. For experiments on Etna hawaiites, this process oxidized the enclosed melt inclusion and increased the homogenization temperature by 100 °C to 150 °C (Sobolev et al. 1990). The net result is a change in the oxidation state of the trapped melt, thus affecting equilibrium between the host phase and the melt inclusion.

We first performed heating experiments similar to those of Varela et al. (2001) with slow heating rates (between 1° to 12° per minute, with slower rates at higher temperatures). The sample was held at the homogenization temperature (~1150 °C) for 20 minutes. Slow-heating experiments were performed in a Vernadsky high-temperature microscope heating stage at Virginia Tech. To avoid oxidation, the samples were heated in an atmosphere of He that had been de-oxygenated by passing over Ti metal at 600 °C. The samples were placed on a mineral plate (olivine, pyroxene, or sapphire) to facilitate their removal from the heating stage following each experiment. With this stage, the sample was visually monitored during the heating experiment.

Homogenization of the melt inclusion was considered complete when daughter crystals were resorbed and the shrinkage bubble was reduced significantly in size. The

Table 1. Representative electron microprobe analyses of melt inclusions in Nakhla augite (NA##) from this study and the nakhlite parental magma composition derived by Treiman and Goodrich (2001), NK01. Size and homogenization temperature (T_h) are also listed for Nakhla melt inclusions.

	Rehomogenized—slow-heating experiments			Rehomogenized—fast-heating experiments					T&G 2001
	NA01a	NA01b	NA02	NA03	NA04	NA05	NA06	NA07	NK01
Size	15 μm	20 μm	45 μm	20 μm	20 μm	30 μm	20 μm	20 μm	–
T_h (°C)	1150	1150	1150	1170	1170	1170	1170	1170	–
SiO_2	56.0	64.4	62.5	47.2	51.2	63.1	54.9	59.2	49.8
TiO_2	1.3	0.62	0.27	0.88	0.84	2.1	0.63	0.34	0.80
Al_2O_3	10.7	13.4	11.0	5.9	7.1	12.3	9.4	9.2	7.5
Cr_2O_3	0.02	0.06	–	–	–	–	–	–	0.10
FeO	14.5	7.5	11.1	26.9	19.6	3.4	15.0	12.3	22.3
MnO	0.39	0.37	0.25	0.71	0.53	0.32	0.43	0.32	0.50
MgO	2.1	0.74	2.5	4.6	4.6	4.0	4.8	4.4	4.6
CaO	8.2	3.5	5.1	10.1	11.2	11.1	9.3	10.1	10.4
NiO	–	–	–	0.07	–	0.0	0.0	–	–
Na_2O	3.4	4.1	3.7	2.3	2.1	1.0	3.6	1.2	1.1
K_2O	2.0	3.6	2.7	0.39	0.70	0.63	0.33	0.66	2.4
P_2O_5	0.65	0.30	0.04	0.09	0.97	0.47	0.42	1.1	0.60
Total	99.2	98.6	99.3	99.1	98.8	98.3	98.8	99.0	100.1
Phases present	glass	glass	glass + oxide	glass	glass	glass + oxide	glass	glass	–

bubbles never completely disappeared, perhaps due to a difference in pressure conditions between the experiment and the original entrapment (Lowenstern 1995). Although this technically represents partial homogenization, Fedele et al. (2003) demonstrated that the melt inclusion composition is not affected by a remnant shrinkage bubble as long as all daughter phases are resorbed. Therefore, we will use the term "homogenized" to describe melt inclusions that have resorbed the daughter crystals, leaving only a glassy phase and the remnants of a bubble. When the inclusion was homogenized completely, the temperature was recorded and the sample was quenched by switching off the power supply, allowing the temperature to drop rapidly. In a Vernadsky heating stage, the average cooling rate during quenching from a maximum temperature of 800 °C in a He atmosphere is up to 500°/sec (Sobolev and Slutskiy 1984). The samples were cooled to several hundred degrees below the melting temperature in a few seconds, thus minimizing the possibility that compositional re-equilibration may have occurred.

In addition, fast-heating experiments were conducted in a 1-atmosphere tube furnace at Virginia Tech. Samples were placed within a platinum capsule with a drop of immersion oil covering the sample to prevent oxidation. The platinum capsule, suspended on a platinum wire, was lowered into a silica glass tube within the furnace. Samples were heated to the desired temperature in about 2 min and held at that temperature for 3 to 5 min, as suggested by Sobolev et al. (1990). The capsule was then removed from the furnace and immediately quenched in water.

Homogenization temperatures were determined by step-heating the samples. The samples were heated to 1100 °C, removed, and the melt inclusions were then examined under a microscope. If a melt inclusion was not completely homogenized, the sample was heated to a temperature 10–20° higher than in the previous step and re-examined. This process was repeated until the melt inclusion was homogenized.

Following the heating experiments, the grains were mounted on the ends of silica glass rods and the (homogenized) melt inclusions were exposed at the surface by carefully polishing down to the level of the melt inclusion (Thomas and Bodnar 2002). The major and minor elemental (Na, K, Mg, Al, Cr, Si, P, K, Ca, Ti, Mn, and Fe) compositions of the melt inclusions and their hosts were measured on a Cameca SX-50 electron microprobe at Virginia Tech (Table 1). Previous work by Fagan et al. (2000) on glass analyses showed that using an accelerating voltage of 15 kV, a current of 2 nA and a defocused beam (5 to 10 μm) minimizes loss of Na, and so these instrumental conditions were employed in this study. In addition, Na was always analyzed first to minimize its loss during exposure to the beam. Counting times range from 40 sec (for K, Na, and Ca) to 70 sec (for Mn and Cr), with all other elements being analyzed for 60 sec.

In this study, eight melt inclusions (each within a separate Nakhla augite grain) were successfully homogenized, remounted, exposed, and analyzed by electron microprobe. Three melt inclusions were homogenized using the slow-heating method and five melt inclusions were homogenized using the fast-heating method. For melt inclusions of sufficient size, multiple analyses were obtained on different spots to assure homogeneity of the glass. Table 1 and related figures show representative compositions as measured using

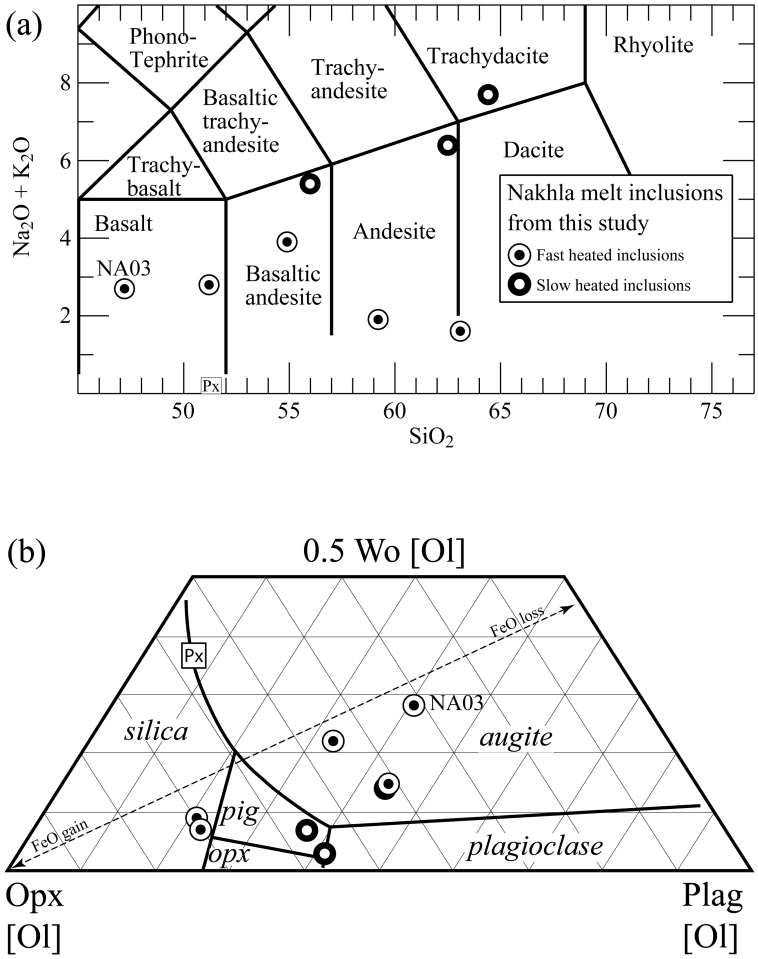

Fig. 3. Melt inclusion compositions from this study on the same diagrams as in Fig. 2. The trend of the homogenized Nakhla inclusion data on the TAS diagram does not point toward the host augite (Px) composition. Incorporating too much host augite would simply move Nakhla melt inclusion compositions toward the host pyroxene composition, suggesting that the most primitive melt inclusions have not re-incorporated excessive amounts of the host phase.

electron microprobe. In addition, Table 1 also presents information regarding the size, homogenization temperature, and phases present in the final quenched inclusion. If a quenched inclusion contains an oxide, this phase probably represents an oxide that was melted during heating, but then re-precipitated during the quenching process.

RESULTS

The composition of rehomogenized melt inclusions from our heating experiments (Table 1) are plotted on the TAS classification diagram (Fig. 3a) and on the olivine projection (Fig. 3b). Melt inclusion compositions range from basalt to dacite, spanning a range of SiO_2 similar to the melt inclusions of Varela et al. (2001). In Fig. 3b, the melt inclusion compositions plot within the augite, pigeonite, and silica fields in both projections. The most primitive (i.e., lowest SiO_2) melt inclusion in Nakhla augite (NA03) plots within the basalt field on the TAS diagram (Fig. 3a) and within the augite field on the olivine projection (Fig. 3b). This melt inclusion plots close to some previous estimates of Nakhla parental melt compositions, as well as the most primitive melt inclusion (GHa) of Varela et al. (2001) (compare Figs. 2 and 3).

For a given silica content, inclusions homogenized by fast-heating show lower abundances of alkalis than inclusions homogenized by slow heating. However, the low alkali contents of the two most evolved (highest silica) fast-heated inclusions may be due to loss of alkalis during heating and/or analyses. Omitting these most evolved inclusions, the remaining inclusions homogenized by both slow- and fast-heating form a distinct trend on the TAS diagram (Fig. 3a). In addition, on an olivine projection diagram (Fig. 3b), these two fast-heated inclusions project into the silica field, suggesting that they should contain both olivine and silica and cannot represent equilibrium compositions.

Should these two high-silica compositions be disregarded? Figure 4 displays melt inclusion compositions from this study as well as those from Varela et al. (2001) on

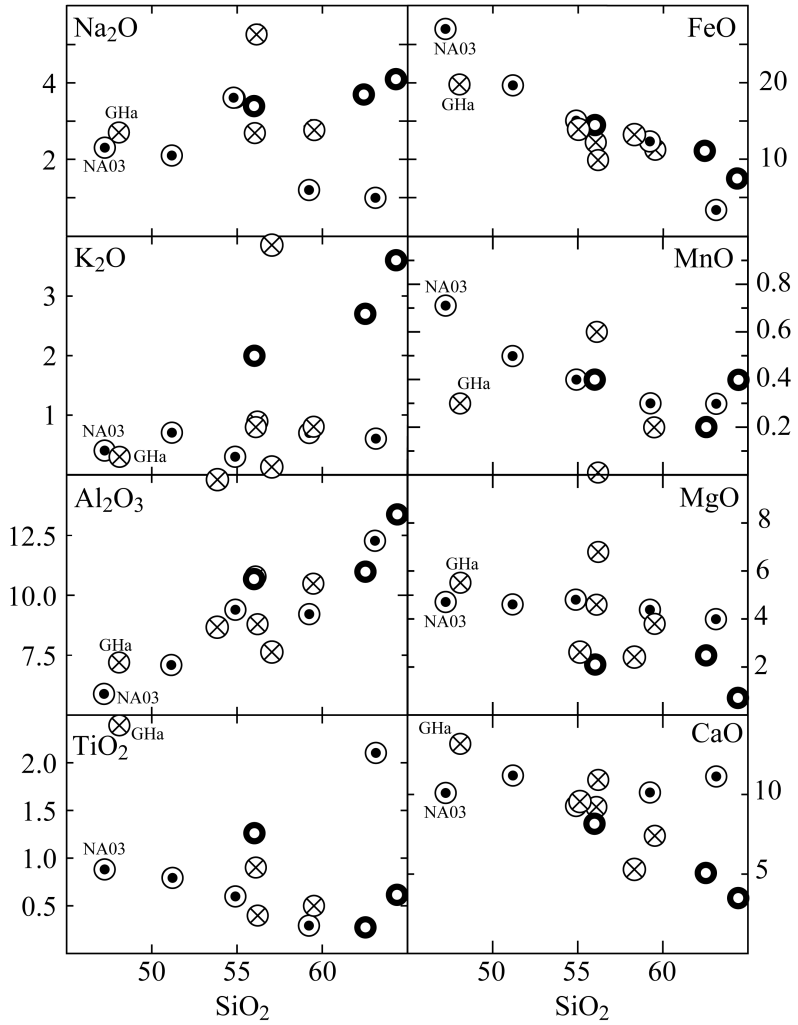

Fig. 4. Harker (wt% oxide) diagrams comparing compositional trends of slowly and rapidly heated melt inclusions in Nakhla pyroxenes from this study and the study of Varela et al. (2001). Symbols for Nakhla melt inclusions as in Figs. 2 and 3 and the most primitive melt inclusions for both studies are labeled. Several oxides show consistent trends regardless of heating rate, whereas others, especially the alkalis and oxides present in lower abundances, show more erratic behavior.

Harker variation diagrams. On these diagrams, these two compositions fall close to linear trends for fast-heated melt inclusions for some oxides (e.g., Al_2O_3, FeO, and MnO) and behave as expected (increasing Al_2O_3, decreasing FeO and MgO) for crystallization of phases observed within Nakhla (e.g., augite, olivine, Fe-Ti oxide). However, for other oxides, the trends of rapidly heated melt inclusions appear flat (K_2O, CaO, and MgO) or do not co-vary as expected (Na_2O decreases while TiO_2 is erratic) (Fig. 4). If we disregard the two high-silica melt inclusions from the fast heating experiments, the trends for the remaining (both fast- and slow-heated) inclusions improve. We conclude that these two points are affected by alkali loss during heating and we will disregard them in the remaining discussion.

The difference in the final homogenization temperature between the slow-heating versus fast-heating experiments was small, with only 20 °C higher homogenization temperatures for the fast-heating experiments (Table 1). In addition, the compositions of melt inclusions that were rapidly heated extend to more primitive compositions compared to those that were heated more slowly (Fig. 4). However, we must also examine whether each melt inclusion was in equilibrium with co-existing minerals at solidus temperatures. Equilibrium temperatures between each melt inclusion and co-existing mineral phases (clinopyroxene, olivine, and plagioclase) were calculated using the PETROLOG software (Sobolev, personal communication; see also http://www.geol.utas.edu.au/~leonid/Petrolog.html). The melt inclusions that were homogenized by the slow-heating technique are in equilibrium with host augite at subsolidus temperatures (<1100 °C), while inclusions that were heated by the fast-heating technique are in equilibrium

Table 2. Mineral compositions measured in nakhlites and produced by MELTS equilibrium and fractional crystallization modeling of NA03 and NK01. Measured compositional ranges include core and rim compositions from the nakhlites.

		Clinopyroxene			Orthopyroxene			Olivine			Plagioclase	
Nakhlites measured		Wo	En	Fs	Wo	En	Fs	Fo	Fa	An	Ab	Or
	Range	22–41	9–40	22–66	2–24	16–38	24–44	14–41	57–86	10–26	60–74	3–30
		Clinopyroxene			Orthopyroxene			Olivine			Plagioclase	
	NA03	Wo	En	Fs	Wo	En	Fs	Fo	Fa	An	Ab	Or
QFM equilibrium model	range	37–43	20–39	19–42	9–10	25–26	64–66	15–34	66–85	15–47	50–76	3–9
	average	40	26	34	10	25	65	21	79	27	67	6
QFM-1 equilibrium model	range	39–42	20–39	20–42	–	–	–	14–34	66–86	14–48	50–77	2–10
	average	41	25	35	–	–	–	19	82	25	68	7
QFM fractional model	range	39–43	8–39	19–50	–	–	–	6–29	71–94	26–48	50–70	3–7
	average	41	27	32	–	–	–	17	83	34	62	4
QFM-1 fractional model	range	41–44	4–39	20–53	–	–	–	2–34	66–98	37–50	48–59	2–4
	average	42	25	33	–	–	–	18	82	42	54	3
		Clinopyroxene			Orthopyroxene			Olivine			Plagioclase	
	NK01	Wo	En	Fs	Wo	En	Fs	Fo	Fa	An	Ab	Or
QFM equilibrium model	range	35–41	21–39	20–42	9–10	26	64–65	17–36	64–84	41–45	47–50	6–10
	average	39	28	34	9	26	65	25	76	43	49	8
QFM-1 equilibrium model	range	34–42	20–40	20–45	10	23–24	66–67	14–45	56–86	45–51	42–47	6–9
	average	39	26	35	10	24	67	22	78	46	46	8
QFM fractional model	range	39–43	0–39	19–58	–	–	–	9–29	71–92	39–49	44–53	7–9
	average	41	19	40	–	–	–	18	82	43	49	8
QFM-1 fractional model	range	40–44	0–40	20–59	–	–	–	3–43	57–97	49–62	33–44	5–7
	average	42	19	39	–	–	–	21	79	55	39	6

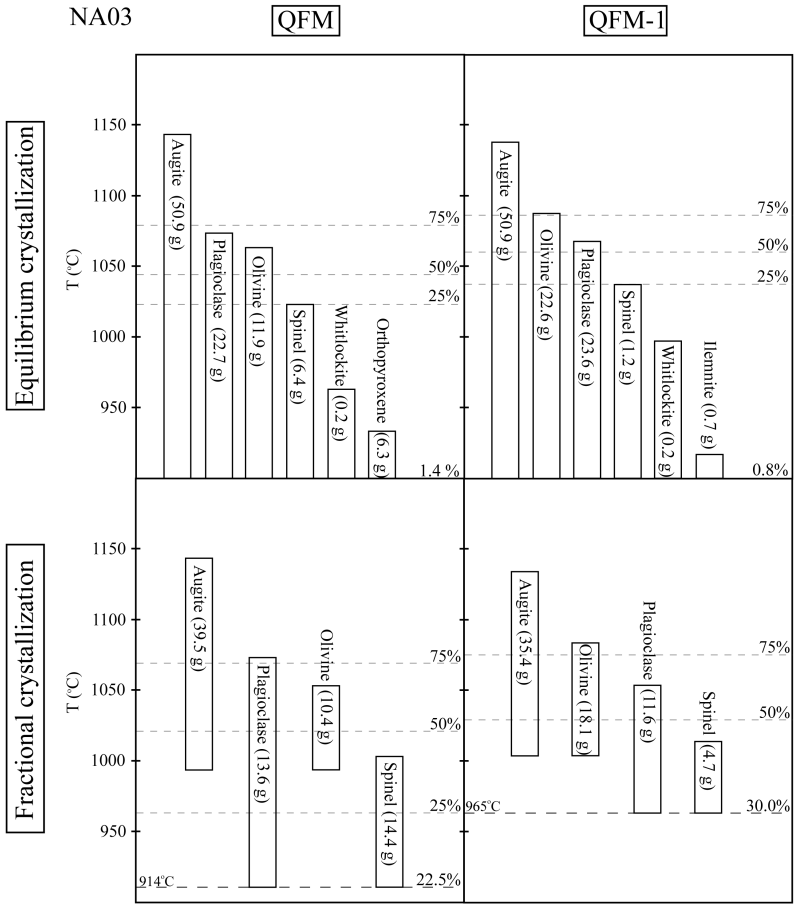

Fig. 5a. Results of MELTS modeling for NA03. Dashed lines (top to bottom) represent temperatures at which there was 75%, 50%, and 25% liquid remaining; the final amount of liquid remaining (at the end of the run) is displayed at the final temperature step for that model. Runs were performed from the liquidus temperature to 900 °C for all conditions except for fractional crystallization, where modeling could only be run to ~914 °C for QFM and ~965 °C for QFM-1 (see discussion section for details). Cumulative amounts of the phases are listed in parentheses after the phase names.

with host augite at higher temperatures (~1140–1160 °C) (Sobolev, personal communication). This suggests that the slow heating inclusions did not remain in equilibrium with the host augite during the heating experiment, while the fast-heating inclusions did remain in equilibrium. Furthermore, only our most primitive melt inclusion, NA03, is saturated with both augite and olivine at high temperatures (Sobolev, personal communication).

DISCUSSION

MELTS Modeling of Melt Inclusion Compositions

Compositions of melt inclusions within Nakhla augite extend into the andesite and trachydacite fields (Fig. 3a). These more evolved compositions may represent pockets of melt that were trapped later in the crystallization history of the rock. Several questions arise when considering this possibility: 1) Did augite continue to crystallize long enough to trap such highly evolved melts? 2) If so, what composition of augite was in equilibrium with the most evolved melt inclusion and how does this match the observed range of augite compositions in Nakhla? 3) Do these melt inclusions fall along a reasonable liquid line of descent? In an attempt to answer these questions, results from the melt inclusion study were compared with those predicted by crystallization modeling using MELTS (Ghiorso and Sack 1995). In addition, measured phase abundances and compositions in Nakhla can be directly compared to those predicted by MELTS to determine which starting composition best matches the Nakhla parent melt composition. We compared the most primitive melt inclusion from this study (NA03) with the currently accepted Nakhla parent magma composition (NK01) of Treiman and Goodrich (2001). These starting compositions were input into MELTS to obtain crystallization sequences for both fractional and equilibrium crystallization (Table 2).

The oxidation state under which Nakhla crystallized is

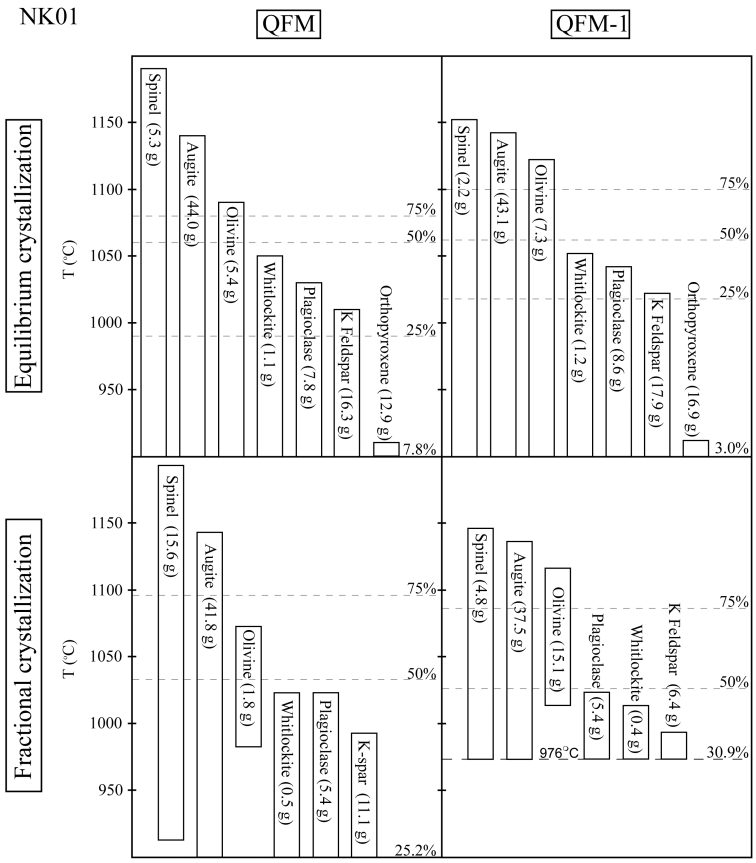

Fig. 5b. Results of MELTS modeling for NK01. Runs were performed from the liquidus to 900 °C except for fractional crystallization at QFM-1, where modeling could only be run to 976 °C (see discussion section for details). Fractional crystallization modeling results have greater amounts of liquid remaining at the end of runs. Dashed lines represent the temperature at which there was 75%, 50%, and 25% liquid remaining and the final amount of liquid remaining is displayed at the final temperature step.

not well constrained. The intrinsic oxygen fugacity measurements of Delano and Arculus (1980) suggest Nakhla crystallized under reducing conditions near the iron-wüstite buffer, but this interpretation is not generally accepted for nakhlites. Moreover, MELTS crystallization modeling at the iron-wüstite buffer does not produce a mineral assemblage that matches the Nakhla mineral assemblage (Slater et al. 2003). Compositions of coexisting Fe-Ti oxides (magnetite and ilmenite) in Nakhla are consistent with an oxidation state of $fO_2 = 10^{-17}$ at 740 °C, just below the quartz-fayalite-magnetite buffer, at QFM-0.4 log units (Reid and Bunch 1975). More recently, Szymanski et al. (2003) constrained the oxygen fugacity of nakhlites using 1) activities of magnetite in spinel and of hematite in ilmenite after Ghiorso and Sack (1991) and 2) the Ca-QUILF model (Andersen et al. 1993). The temperature and log fO_2 determined by these two methods were 1) T = 824 °C and QFM-0.20 log units and 2) T = 795 °C and QFM + 0.14 log units, with the absolute error of the oxygen fugacity estimates of ±0.5 log units.

We ran MELTS at both QFM and QFM-1 as bounding conditions for the modeling. We first obtained the liquidus temperature for an individual run and then began crystallization runs 10 °C above the liquidus. Equilibrium crystallization was modeled in 10° temperature steps, stopping at 900 °C. Fractional crystallization was also modeled in 10° intervals; however, it was not always possible to continue fractional crystallization down to 900 °C, possibly due to problems when applying the MELTS program outside its calibrated compositional range (i.e., for Fe-rich melts, as noted by Hale et al. [1999]). In these cases, modeling was terminated at higher temperatures.

Duration of Augite Crystallization

The crystallizing phases and corresponding temperature ranges for models using NA03 from this study are shown in Fig. 5a. In equilibrium crystallization models, augite crystallized through all time steps, whereas for fractional crystallization models, augite stopped crystallizing when 50%–25% liquid remained. All average augite compositions fall within the measured range of Nakhla augites and the model compositional ranges for augites are similar to those observed in nakhlites (Table 2 and Fig. 6a).

For models using NK01 from the study of Treiman and

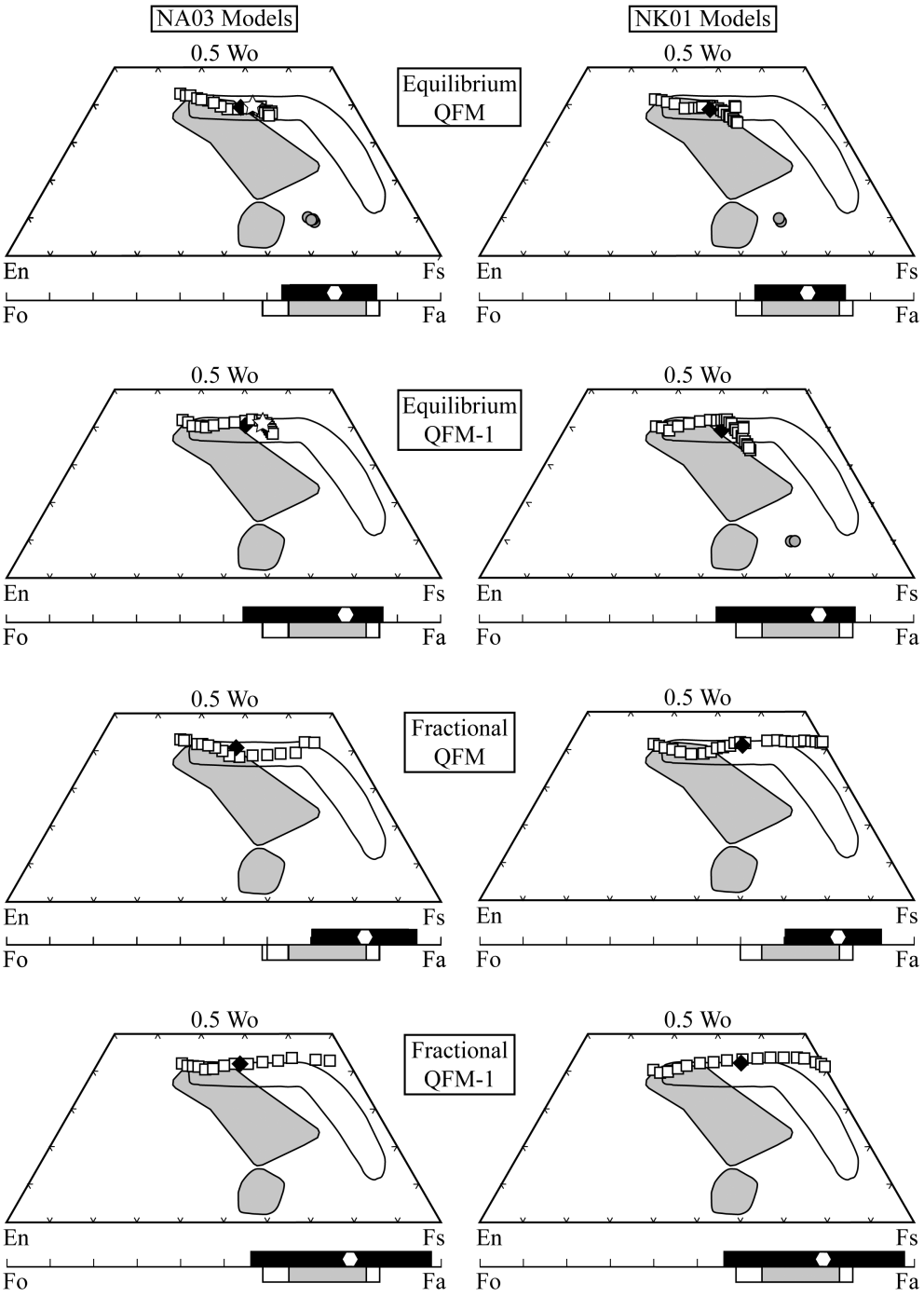

Fig. 6a. Pyroxene and olivine compositions resulting from MELTS crystallization models for NA03 and NK01. On the pyroxene quadrilateral, open squares represent augite compositions and filled circles represent orthopyroxene compositions. The average augite composition is shown by a black diamond. Gray areas enclose pyroxene compositions measured in most nakhlites (Harvey and McSween 1992b), whereas the outlined area encloses pyroxene compositions analyzed in the unannealed nakhlite Northwest Africa (NWA) 817 (Sautter et al. 2002). On the olivine bar, the upper black box displays the range of compositions produced by the model, with the average olivine composition represented by the polygon. The gray box displays the range of measured olivine compositions in most nakhlites (Harvey and McSween 1992b), whereas the open box displays the large range of olivine compositions in NWA 817 (Sautter et al. 2002). On the NA03 equilibrium crystallization at QFM and at QFM-1 quadrilaterals, the open stars represent the augite composition produced by the MELTS model for liquids similar in composition to our most evolved melt inclusion.

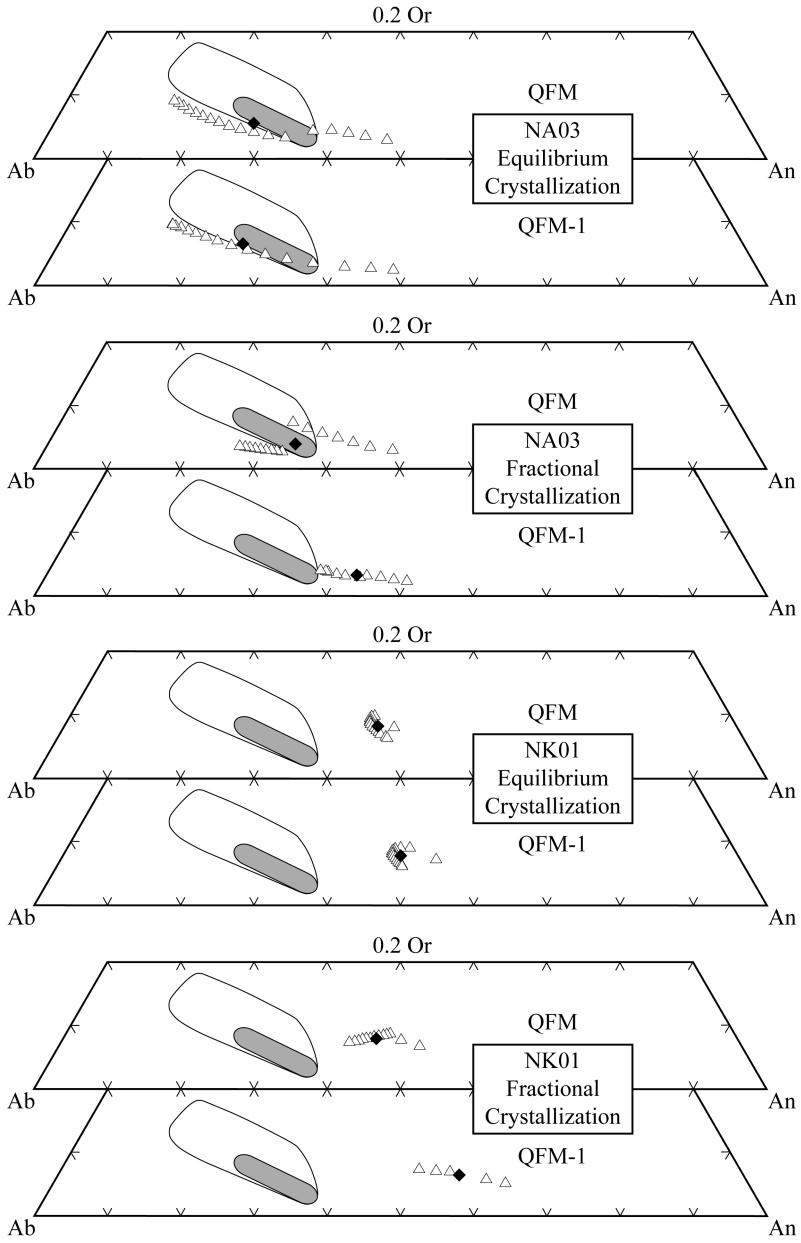

Fig. 6b. Plagioclase compositions from MELTS crystallization models for NA03 and NK01. Triangles represent plagioclase compositions from the model and the black diamond represents the average of these plagioclases. Gray area outlines measured plagioclase compositions in most nakhlites (Berkley et al. 1980), whereas the outlined area includes plagioclase compositions measured in NWA 817 (Sautter et al. 2002).

Goodrich (2001), the phases that crystallized and the temperature ranges over which they crystallized are summarized in Fig. 5b. Note that augite continued to crystallize until the last temperature step for all models. The average augite compositions from both equilibrium and fractional crystallization fall within the measured range of augite compositions (Table 2 and Fig. 6a).

An important result of these models is that augite (similar in composition to that found in nakhlites) continues to crystallize from a liquid as evolved as rhyolite, suggesting that it is possible for the Nakhla augite to been in equilibrium with the more evolved melt inclusions. In addition, augite in equilibrium with evolved liquids (65 wt% SiO_2) is similar in composition to augite from the unannealed nakhlite. Therefore, the more evolved melt inclusions may represent pockets of liquid that were trapped as melt inclusions within augite at various times during the crystallization history.

Model Augite Composition Compared to Nakhlite Augites

The augite composition in equilibrium with evolved liquids in these calculations (e.g., ~65 wt% SiO_2, similar to the most evolved melt inclusion) matches the measured augite

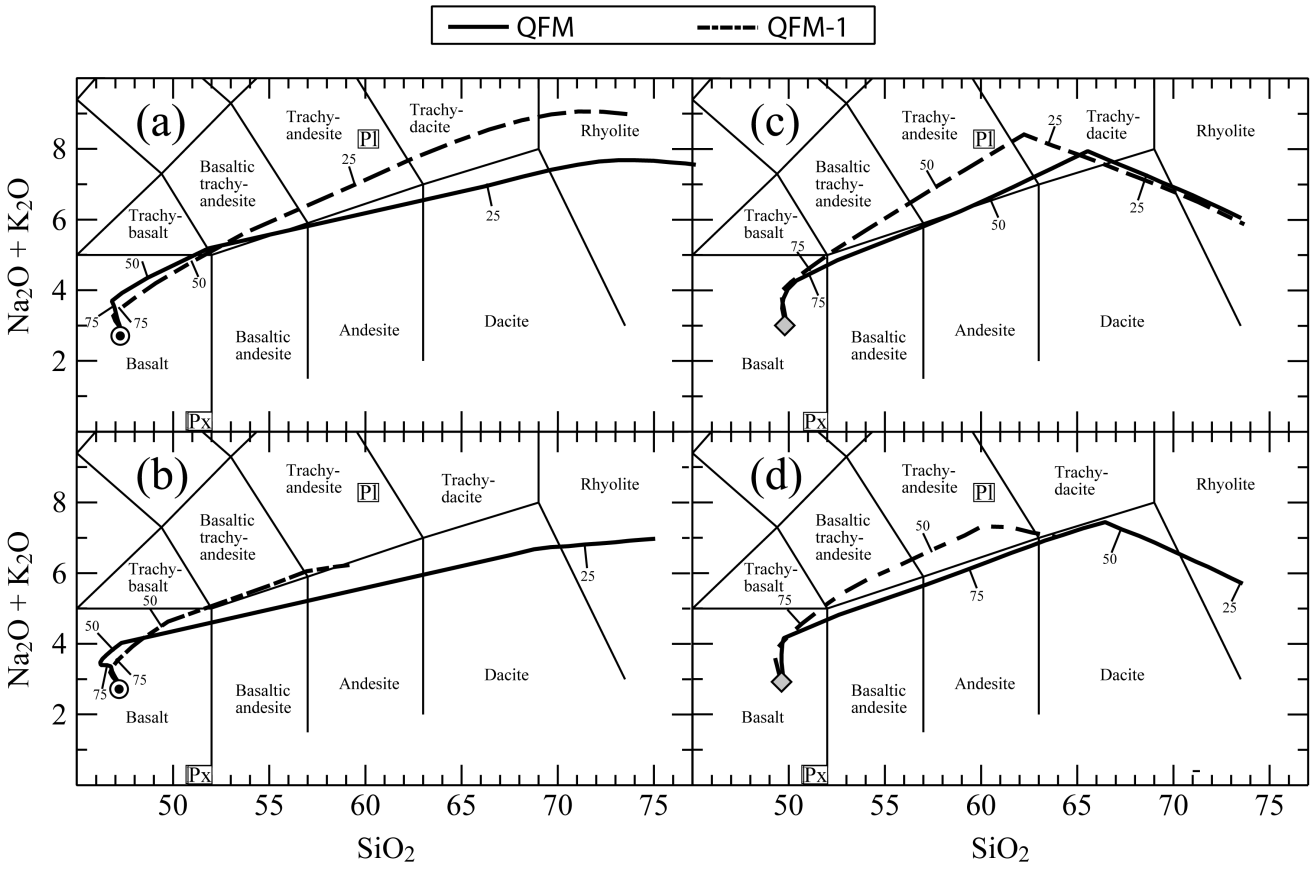

Fig. 7. Calculated evolutionary paths of liquid compositions produced from crystallization modeling in MELTS plotted on the TAS diagram. Hatch marks along paths indicate 75%, 50%, and 25% liquid remaining, unless otherwise indicated. Solid lines represent crystallization at QFM, whereas dashed lines represent crystallization at QFM-1. Starting composition symbols as in Figs. 2 and 3. a) Equilibrium crystallization of NA03; b) Fractional crystallization of NA03 (QFM-1 path stops at 30% liquid remaining); c) Equilibrium crystallization of NK01; d) Fractional crystallization of NK01 (QFM-1 path stops at 31% liquid remaining).

compositions in some nakhlites. The augite composition in equilibrium with this liquid is plotted as an open star on the pyroxene quadrilateral for equilibrium crystallization of NA03 at QFM and at QFM-1 (Fig. 6a). This augite composition plots within the field of augite composition in the unannealed nakhlite, Northwest Africa (NWA 817) (Sautter et al. 2002) for both oxidation states (Fig. 6a). Other nakhlites have experienced various degrees of subsolidus annealing (Harvey and McSween 1992b). The model pyroxenes have Fe/Mg ratios ranging from 0.48–2.10 (QFM) and 0.51–2.16 (QFM-1), similar to the observed Fe/Mg range for annealed nakhlites (core to rim ranges: 0.55 to 1.97 [Friedman Lentz et al. 1999; McSween and Treiman 1998]) and roughly within the Fe/Mg ratio range for the unannealed nakhlite NWA 817 (core to rim range: 0.61 to 7.42 [Sautter et al. 2002]).

Model Liquid Lines of Descent Versus Measured Melt Inclusion Compositions

The calculated liquid lines of descent from MELTS crystallization modeling of NA03 and NK01 are shown in Figs. 7a–d. Each plot shows the evolution of the liquid path at both QFM and QFM-1 on TAS diagram. We use these two paths to define a zone of predicted compositions for liquids at various degrees of crystallization. Thus, if representative pockets of this liquid were trapped as melt inclusions during crystallization of the melt, these inclusions should be distributed along this zone.

The liquid paths for both starting compositions straddle the sub-alkaline/alkaline border on the TAS diagram (Figs. 7a–d). In general, for low silica contents (e.g., in the basalt to basaltic andesite range), the alkali abundances of these paths are higher than measured in Nakhla melt inclusions having the same SiO_2 composition. However, at higher silica contents, the Nakhla melt inclusions match more closely the predicted alkali abundances. In general, these liquid paths define the regions where measured melt inclusion compositions plot (cf. Figs. 2 and 3), suggesting that the melt inclusions could represent pockets of liquid that were trapped during progressive crystallization of the nakhlite parent melt. An alternative interpretation is that all inclusions, other than NA03, were modified after trapping by necking down and that the similarity between inclusion compositions and the modeled liquid lines of descent is fortuitous. This interpretation may be supported by the range in incompatible

elements (Ti, K, P) present in the melt inclusion data. However, no petrographic evidence for necking down was observed.

Comparison of Model Phase Abundances and Compositions with the Nakhlites

Finally, we look at how well the MELTS crystallization models for the two starting compositions (NA03 and NK01) match the crystallization sequence inferred for the nakhlites. Both augite and olivine are inferred to have been early crystallizing phases, although there is disagreement as to which began to crystallize first (Harvey and McSween 1992a; Mikouchi et al. 2003; Treiman 1986, 1993; Wadhwa and Crozaz 1995). Low-Ca pyroxene occurs as overgrowths on augite and as a replacement of olivine and augite (Harvey and McSween 1992a; Treiman 1990). Feldspars, oxides (titanomagnetite and ilmenite), and sulfides occur within the mesostasis and represent late-stage crystallization products (Berkley et al. 1980).

All crystallizing phases and corresponding temperature ranges for models using NA03 are shown in Fig. 5a. Differences in oxidation state and type of crystallization (equilibrium versus fractional) had a greater effect on the appearance of phases than for NK01 models (Fig. 5b). Equilibrium crystallization produced augite, olivine, spinel, plagioclase, and whitlockite. Under more oxidizing conditions orthopyroxene crystallized, whereas ilmenite crystallized under more reducing conditions. Plagioclase appeared before olivine and spinel during equilibrium crystallization at QFM. Fractional crystallization modeling produced augite, plagioclase, olivine and spinel. Oxidation state affected the temperature stability range of the phases and their order of appearance, but did not change the phase assemblage.

As mentioned above, the NA03 models produce average augite compositions that fall within the measured range of nakhlite augites. Furthermore, the model compositional ranges are similar to those observed in nakhlites (Table 2 and Fig. 6a). The average orthopyroxene composition is more Fe-rich than the range of measured orthopyroxene compositions (Table 2 and Fig. 6a). In fact, the model compositional ranges are very narrow and extend to more Fe-rich compositions when compared to the observed ranges. All average olivine compositions fall within the measured range, but model olivine compositional ranges tend to exceed the observed compositional range, especially for fractional crystallization models (Table 2 and Fig. 6a). Average plagioclase compositions (Fig. 6b) fall within the measured range in nakhlites, with the exception of the average plagioclase composition for fractional crystallization at QFM-1. All models have plagioclases that extend to more calcic compositions than the measured compositional range. Model plagioclase compositions for fractional crystallization at QFM-1 are not consistent with the measured compositional range (Table 2 and Fig. 6b).

All models of NK01 predict spinel, augite, olivine, whitlockite, plagioclase and K-feldspar (Fig. 5b). However, spinel crystallizes before both augite and olivine in all models. Orthopyroxene only formed (late) during equilibrium crystallization. The oxidation state affected the temperature at which the phases appeared, but not their presence in the system. The appearance of a phase at a higher temperature resulted in production of a greater quantity of that phase. In fractional crystallization models, olivine crystallization ceased at elevated temperatures (980 °C to 1010 °C), but did not necessarily decrease the amount of olivine produced (e.g., at QFM-1, 15.1 g of olivine crystallized).

As mentioned above, NK01 models produced average augite compositions from both equilibrium and fractional crystallization that fall within the measured range of augite compositions in nakhlites (Table 2 and Fig. 6a). The average orthopyroxene compositions are too Fe-rich and display very narrow compositional ranges relative to measured compositions in the nakhlites (Table 2 and Fig. 6a). All average olivine compositions fall within the measured range (Table 2 and Fig. 6a). However, model olivine compositional ranges tend to exceed the measured range, especially for fractional crystallization at QFM-1. All model plagioclase compositions for NK01 models are significantly more calcic than the measured compositional range (Table 2 and Fig. 6b).

MELTS crystallization modeling provides insight into the Nakhla parent melt composition and the conditions under which it crystallized. Perhaps most telling is that, regardless of the type of crystallization within a plausible range of oxidation state, both NA03 and NK01 co-crystallize augite and olivine from a single parent melt. Disequilibrium between augite and olivine in Nakhla has been documented previously (Harvey and McSween 1992a; Treiman 1986) and explained as either the olivines being xenocrysts (Treiman 1986) or as a result of varying degrees of re-equilibration of both olivine and augite grains near solidus temperatures (Harvey and McSween 1992a). According to MELTS crystallization modeling, the disequilibrium observed between augite and olivine Fe/Mg ratio must then indicate subsequent re-equilibration of olivine (Harvey and McSween 1992a) and lesser re-equilibration of augite. This is consistent with the findings from NWA 817, an unannealed nakhlite. The olivine in NWA 817 exhibits strong zoning from core to rim (e.g., Fo56 to Fo86 in one grain) and extend to more fosteritic compositions relative to other nakhlites (Fig. 6a) (Sautter et al. 2002). Olivine zoning indicates that this sample spent a shorter time near the solidus temperature, and underwent less re-equilibration than other nakhlites. Clinopyroxene core compositions are very similar to those measured in other nakhlites, suggesting that the cores of augite in all nakhlites are relatively unaltered (Sautter et al. 2002).

Equilibrium crystallization models produce augite and olivine compositions that match the measured compositions

Table 3. $K_D(Fe\text{-}Mg)_{augite\text{-}glass}$ values[a] for several proposed parental magma compositions.

	NA03[b]	GH(6)[c]	GHa[d]	GHa[d]–3% augite	NK01[e]
FeO/MgO_{glass}	5.79	2.73	3.56	3.75	4.85
FeO/MgO_{augite}	1.47	1.09	1.09	1.09	1.09
$K_D(Fe\text{-}Mg)_{augite\text{-}glass}$	0.254	0.399	0.307	0.291	0.226

[a]Note: $K_D(Fe\text{-}Mg)_{augite\text{-}glass}$ was determined experimentally by Longhi and Pan (1988) to range from 0.293 to 0.179. The FeO/MgO_{augite} for melt inclusions studies come from host pyroxene compositions of the respective studies, whereas FeO/MgO_{augite} for the other estimates comes from a representative augite core composition from Treiman (1990).
[b]The most primitive melt inclusion from this study.
[c]Average composition of six melt inclusion from the study of Varela et al. (2001).
[d]The most primitive melt inclusion from the study of Varela et al. (2001).
[e]Most recent nakhlite parent magma composition from the study of Treiman and Goodrich (2001).

Table 4. Calculations of potential boundary layer problems for a basaltic liquid after Lu et al. (1995).[a]

Parameters used in calculations:											
Growth rate[b]	V (cm/s)			2.05 e -08							
		1100 °C				1200 °C					
Diffusivity[c] (cm^2/s)	D (Ca^{2+})	1.41 e -09				4.37 e -09					
	D (Mg^{2+})	2.14 e -09				6.76 e -09					
	D (Fe^{2+})	1.91 e -09				5.62 e -09					
	D (Al^{3+})	2.75 e -09				8.91 e -09					
	D (Ti^{4-})	2.14 e -09				6.76 e -09					
Augite/liquid partition coefficients[d]	$k(CaO)_{aug\text{-}liq}$			1.41 ± 0.1							
	$k(MgO)_{aug\text{-}liq}$			1.9 ± 0.1							
	$k(FeO)_{aug\text{-}liq}$			0.43 ± 0.08							
	$k(Al_2O_3)_{aug\text{-}liq}$			0.13 ± 0.01							
	$k(TiO_2)_{aug\text{-}liq}$			0.17 ± 0.03							
Growth at 1100 °C:						Growth at 1200 °C :					
x (microns)	C_x (Ca)	C_x (Mg)	C_x (Fe)	C_x (Al)	C_x (Ti)	x (microns)	C_x (Ca)	C_x (Mg)	C_x (Fe)	C_x (Al)	C_x (Ti)
0	0.7	0.5	2.3	7.7	5.9	0	0.7	0.5	2.3	7.7	5.9
1	1.0	1.0	1.0	1.0	1.0	1	1.0	1.0	1.0	1.7	1.2
2	1.0	1.0	1.0	1.0	1.0	2	1.0	1.0	1.0	1.1	1.0
3	1.0	1.0	1.0	1.0	1.0	3	1.0	1.0	1.0	1.0	1.0
4	1.0	1.0	1.0	1.0	1.0	4	1.0	1.0	1.0	1.0	1.0
5	1.0	1.0	1.0	1.0	1.0	5	1.0	1.0	1.0	1.0	1.0
10	1.0	1.0	1.0	1.0	1.0	10	1.0	1.0	1.0	1.0	1.0
15	1.0	1.0	1.0	1.0	1.0	15	1.0	1.0	1.0	1.0	1.0
20	1.0	1.0	1.0	1.0	1.0	20	1.0	1.0	1.0	1.0	1.0
25	1.0	1.0	1.0	1.0	1.0	25	1.0	1.0	1.0	1.0	1.0

[a]Note: The calculated concentration is the concentration of component i ($C_x(i)$) at distance x from the crystal-melt interface equal to some multiple (n) of the original concentration of component i ($C_o(i)$). [$C_x(i) = n * C_o(i)$].
[b]Friedman Lentz et al. (1999).
[c]Calculated after Donaldson (1975).
[d]k-values calculated from the experiments of Longhi and Pan (1988).

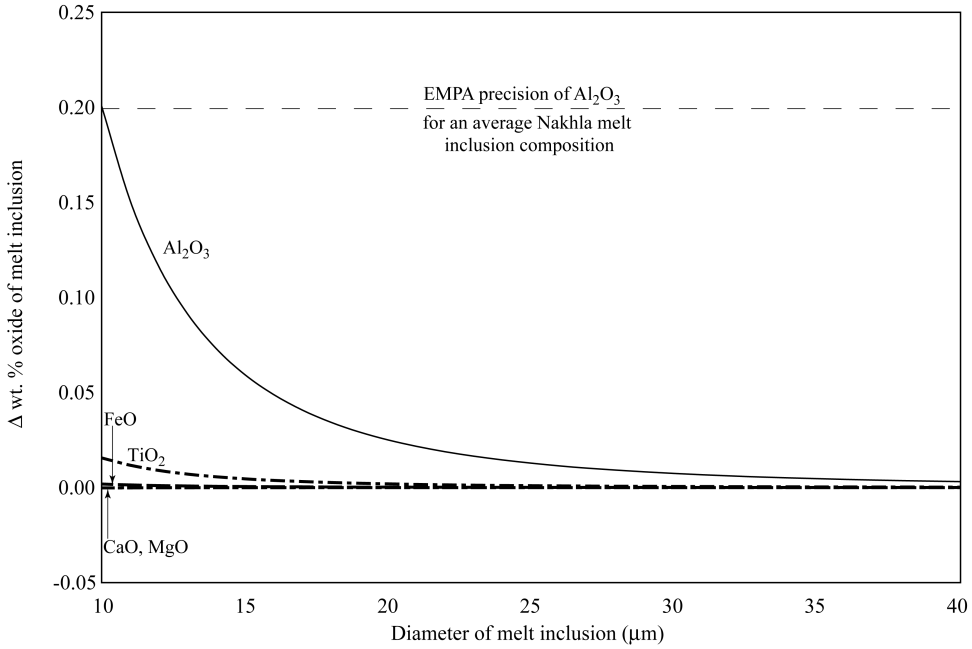

Fig. 8. Evaluation of the magnitude of the boundary layer effect on the composition of melt inclusions of variable sizes, as suggested by Treiman (2003). The difference in oxide abundance caused by the boundary layer is below the detection limits of this method for all oxides, except Al_2O_3. For melt inclusions with a diameter of ~16 μm and larger, no compositional effect is detectable by electron microprobe analysis.

more closely (Table 2 and Figs. 6a–b). Both starting compositions produced reasonable pyroxene and olivine compositions; however, the NK01 models failed to produce plagioclase compositions that match any measured nakhlite composition, and they predict very early crystallization of spinel, which has not been seen in nakhlites. The NA03 model plagioclase compositions agree with measured plagioclase, so we suggest that NA03 may be more representative of the Nakhla parental melt composition.

In the crystallization models of NA03, plagioclase appears before olivine in both equilibrium and fractional crystallization models at QFM. However, in the crystallization models at QFM-1, olivine appears before plagioclase, providing a better match to the inferred order of appearance (Fig. 5a). Between the two models at QFM-1, equilibrium crystallization provides a better match to the phases present in nakhlites (Fig. 5a) as well as predicts model plagioclase that correspond more closely to the measured plagioclase compositions in nakhlites (Fig. 6b). Therefore, we suggest that equilibrium crystallization of NA03 at QFM-1 best represents the conditions of crystallization and parental melt composition of the nakhlites.

Water Content of the Nakhla Parent Magma

In the study of Sobolev et al. (1990), melt inclusions in Etna hawaiites showed a large variation in homogenization temperatures (150 °C) as a function of heating rate due to high water contents (estimated to be about 1 wt%). The relatively small variation in the homogenization temperature between the fast- and slow-heating experiments on Nakhla melt inclusions is consistent with a low water content of the nakhlite parental melt. The higher homogenization temperatures for more primitive melt inclusions that were heated rapidly suggest that these are the earliest melts that were trapped. A low water content for the Nakhla parent melt is consistent with the absence of hydrous minerals (e.g., hydrous amphiboles, mica) in melt inclusions. Such phases have been found in other types of martian meteorites (Johnson et al. 1991; Treiman 1985), and have been used to infer higher magmatic water contents (Johnson et al. 1991; McSween and Harvey 1993).

Apparent Disequilibria Between Melt Inclusions and Nakhla Augite and Olivine

In melt inclusion studies, the most primitive inclusion composition is normally chosen to represent the parental melt composition. In contrast, Varela et al. (2001) regarded their most primitive melt inclusion composition (GHa) as anomalous, because it did not cluster with the other measured melt inclusions. Based on its composition, shape, and bubble size, this basaltic melt inclusion was interpreted to be a product of necking, whereby an inclusion becomes divided into two inclusions, each of which may no longer represent the original trapped melt composition. However, Figs. 2, 3, and 4 show that GHa plots close to both the previous estimates for the parental melt of Nakhla and our most primitive melt inclusion (NA03).

Instead, Varela et al. (2001) presented their average melt

inclusion composition GH(6) as a representative composition and suggested that it was not in equilibrium with the host augite or co-existing olivine. However, their melt inclusion data show a large standard deviation for this average composition (Fig. 2) and no individual melt inclusion compositions from that study were evaluated to determine if they were in equilibrium with host augite or the co-existing olivine.

Table 3 displays calculated $K_D(Fe\text{-}Mg)_{augite\text{-}liquid}$ for several parental melt compositions discussed in this paper. Longhi and Pan (1988) calculated a range of K_D(Fe-Mg) from augite-glass pairs in crystallization experiments, ranging from 0.293 to 0.179. The average composition GH(6) of Varela et al. (2001) has the largest K_D(Fe-Mg) value, but the K_D(Fe-Mg) for inclusion GHa from Varela et al. (2001) is much closer to the acceptable range. In fact, by subtracting only 3% of their average augite composition from the melt inclusion GHa, the melt composition is brought into equilibrium with its host. This suggests that more augite has been dissolved into the melt than was originally precipitated onto the walls of the melt inclusion.

The K_D(Fe-Mg) of augite-liquid for NA03 falls within the range of K_D(Fe-Mg) values indicated by the crystallization experiments of Longhi and Pan (1988). This is consistent with an interpretation in which the correct amount of augite (i.e., the amount plated out on the walls of the inclusion following entrapment) was resorbed back into the melt inclusion. NA03 is the most primitive (i.e., earliest trapped) melt inclusion among the inclusions from both melt inclusion studies and is in equilibrium with both host augite and olivine at high temperature (~1150 °C). Therefore, NA03 is considered to be the melt inclusion most representative of Nakhla's parental melt composition.

In discussion of the results of Varela et al. (2001), Treiman (2003) suggested the disequilibrium between melt inclusions and host augite might be due to a boundary layer effect. This occurs when the melt adjacent to the growing crystal becomes enriched in components that diffuse slowly towards the growing crystal or that are incompatible with respect to the growing phase (Anderson 1974; Bacon 1989). Treiman (2003) reasoned that excess SiO_2, Al_2O_3, TiO_2, and Na_2O in small melt inclusions would be expected due to boundary layer problems. However, more recent work has shown that, with the exception of the smallest inclusions and the fastest crystal growth rates, the compositions of melt inclusions are not affected by boundary layers (Thomas et al. 2002).

Our calculations of boundary layer effects (after Lu et al. 1995; using constants from Donaldson 1975 and Friedman-Lentz et al. 1995) reveal that gradients would exist for Ca, Fe and Mg at the crystal-melt boundary, but would extend only 1 μm into the melt (Table 4). Gradients would exist out to 2 μm for Ti and out to 3 μm for Al. The effect of this gradient on the bulk composition of the melt inclusion can also be calculated (Lu et al. 1995). The smallest inclusion that can be analyzed by our technique is 10 μm, so we will discuss compositional changes due to a boundary layer effect for a 10 μm inclusion as a worst-case scenario; it should be noted that all homogenized inclusions from this study with the exception of one (~15 μm) were >20 μm.

For a 10 μm melt inclusion, the boundary layer effect would not produce measurable differences in the concentration of CaO, FeO, or MgO, but might produce measurable changes in Al_2O_3 (+0.20 wt%) and TiO_2 (+0.02 wt%). For major elements, the precision of electron microprobe analyses is generally ±2% relative; for minor elements, the precision is ±5–10% relative. In this study, the average Nakhla melt inclusion contained 9.9 wt% Al_2O_3, so the precision of that analysis would ±0.20 wt%. Therefore, only the enrichment in Al_2O_3 in a 10 μm melt inclusion would be near measurable levels. As can be seen in Fig. 8, the increase in Al_2O_3 abundance in a melt inclusion due to an Al_2O_3-enriched boundary layer quickly decreases as melt inclusion size increases. Compositional errors for Al_2O_3 resulting from boundary layer processes would be undetectable in all melt inclusions 10 μm and larger.

Finally, the lack of equilibrium between augite-hosted melt inclusions and co-existing olivine is expected. Olivines in Nakhla are no longer in equilibrium with co-existing augite, probably due to variable degrees of subsolidus equilibration of these two phases (Harvey and McSween 1992a). Therefore, the Nakhla olivine composition should not be in equilibrium with the melt inclusions located within co-existing augite cores.

Igneous Origin for Nakhlites

MELTS modeling demonstrates that equilibrium crystallization of a basaltic parental melt similar in composition to NA03 or NK01 predicts extended crystallization of augite and olivine, so that these phases might trap highly evolved melt inclusions. In addition, the melt inclusion compositions match well with liquid paths predicted by MELTS crystallization modeling for a parent melt similar in composition to NA03 or NK01.

There is no reason to argue, as did Varela et al. (2001), that the melt inclusions in nakhlites require a non-igneous origin for these meteorites. The apparent disequilibrium between Nakhla augite, olivine and the augite-hosted melt inclusions and the erratic behavior of the alkalis do not rule out an igneous origin for Nakhla. The apparent disequilibrium is relatively small for the most primitive melt inclusion from the study of Varela et al. (2001) and is easily corrected by subtracting small amounts of the host augite. This suggests that the previous study dissolved too much augite (more than that crystallized on the walls of the inclusion following entrapment), which would create the appearance of disequilibrium between the melt inclusion and the host augite. In addition, since olivines in Nakhla are no longer in equilibrium with co-existing augite (e.g., Harvey and

McSween 1992a; Treiman 1986), the Nakhla olivine composition should not be in equilibrium with the augite-hosted melt inclusions (although the inclusions should be in equilibrium with an appropriate olivine composition). Finally, the variability of alkalis in Nakhla melt inclusions reported by Varela et al. (2001) may result from experimental or analytical problems. In particular, the validity of an augite-hosted melt inclusion that contains less than 1 wt% alkalis (Fig. 2a) may need to be re-examined. According to distribution coefficients calculated from the experimental work of Longhi and Pan (1988), a liquid in equilibrium with Nakhla augite must contain more than 1 wt% alkalis. We did not observe as much scatter in the alkali contents of Nakhla melt inclusions in our study.

SUMMARY

Partly crystallized melt inclusions in the Nakhla meteorite have been studied in an attempt to reconcile differences among estimated compositions of the Nakhla parental melt. We selected inclusions hosted in augite rather than olivine because Nakhla olivines re-equilibrated during annealing and because olivine-hosted inclusions are known to re-equilibrate easily during heating, both in nature and in the laboratory. We experimentally homogenized melt inclusions using both slow- and fast-heating techniques. The compositions of melt inclusions generally agree with the results of Varela et al. (2001). From this study, we have learned:

1. Melt inclusion compositions are consistent with Nakhla being an igneous rock, the parent melt composition and crystallization history of which clearly reflect planetary (martian) igneous processes.
    a. Calculations of the Fe-Mg equilibrium distribution coefficient ($K_D(Fe\text{-}Mg)_{augite\text{-}liquid}$) values for measured melt inclusion compositions are consistent with the range determined by crystallization experiments of (Longhi and Pan 1988).
    b. The hypothesis of Varela et al. (2001) that Nakhla melt inclusions represent heterogeneously trapped liquids and solids not formed through igneous processes is unwarranted. Their conclusion was based on an assumption that Nakhla's parent melt could be represented by an average of all their melt inclusions. We argue instead that the parent melt is approximated by their most primitive melt inclusion, GHa.
    c. Calculations of the effect of boundary layer diffusion on small melt inclusions for the Nakhla parent melt (as suggested by Treiman 2003) demonstrate that any compositional effect would not be detectable by electron microprobe analyses.
2. Melt inclusions are distributed along MELTS-calculated liquid lines of descent for proposed Nakhla parental melts (NA03 or NK01), suggesting the inclusions may represent liquids trapped at various points along a fractionation sequence.
    a. In MELTS models at QFM-1, the calculated equilibrium crystallization sequence for NA03 was augite, olivine, plagioclase, spinel, whitlockite and ilmenite, consistent with the crystallization sequence inferred from Nakhla petrography.
    b. The composition of host augite predicted by MELTS does not change significantly during the crystallization interval corresponding to the melt inclusions and is consistent with measured augite composition.
    c. Co-crystallization of augite and olivine in these crystallization models supports the hypothesis that olivines in Nakhla re-equilibrated during subsolidus annealing (Harvey and McSween 1992a) rather than the olivine being xenocrystic (Treiman 1986).
3. Melt inclusion NA03 most closely represents the composition of the original parental melt from Nakhla.
    a. Our most primitive melt inclusion composition (NA03) has the lowest SiO_2 and a high Mg# and relatively high homogenization temperature (1170 °C). We infer that this basaltic composition most closely represents the Nakhla parent melt. This composition is very similar to NK01, derived by Treiman and Goodrich (2001), and to GHa, the most primitive melt inclusion of Varela et al. (2001).
    b. Compositions of augite and olivine for both NA03 and NK01 crystallization models match compositions observed in nakhlites. However, NK01 models crystallize spinel very early (not observed in Nakhla) and plagioclase that is more calcic than measured in nakhlites. Thus, we suggest that NA03 may be a better parental melt composition.
    c. The small variation in homogenization temperatures between slow- and fast-heated melt inclusions suggests that the Nakhla parental melt had a low water content.

Acknowledgments–We are grateful to The British Museum of Natural History, through the Meteorite Working Group, for providing samples, and to Jay Thomas, Charles Farley, Luca Fedele, Mercedes Gonzalez-Student, and Jim Student for their assistance and advice regarding laboratory work. This work benefited from discussions with or reviews by Rachel Lentz, Mark Ghiorso, Cyrena Goodrich, Leonid Danyushevsky, Allan Treiman, Richard Sacks, Ralph Harvey, Steve Singletary, and Alex Sobolev; Gretchen Benedix and Bob Tracy provided support in acquiring glass analyses. This study was supported by NASA Cosmochemistry grants NAG5-11744 to H. Y. M. and NAG5-10733 to R. J. B. and awards from the UT Scholarly Activities Research Incentive Fund and the Southeast Section of the Geological Society America to K. R. S.

Editorial Handling—Dr. Cyrena Goodrich

REFERENCES

Andersen D. J., Lindsley D. H., and Davidson P. M. 1993. QUILF: A Pascal program to assess equilibria among Fe-Mg-Mn-Ti oxides, pyroxenes, olivine, and quartz. *Computers & Geosciences* 19: 1333–1350.

Anderson A. T. Jr. 1974. Evidence for a picritic, volatile-rich magma beneath Mt. Shasta, California. *Journal of Petrology* 15:243–267.

Anderson A. T. Jr. 1979. Water in some hypersthenic magmas. *Journal of Geology* 87:509–531.

Bacon C. R. 1989. Crystallization of accessory phases in magmas by local saturation adjacent to phenocrysts. *Geochimica et Cosmochimica Acta* 53:1055–1066.

Berkley J. L., Keil K., and Prinz M. 1980. Comparative petrology and origin of Governador Valadares and other nakhlites (abstract). 11th Lunar and Planetary Sciency Conference. pp. 1089–1102.

Danyushevsky L. V., McNeill A. W., and Sobolev A. V. 2002a. Experimental and petrological studies of melt inclusions in phenocrysts from mantle-derived magmas: An overview of techniques, advantages and complications. *Chemical Geology* 183:5–24.

Danyushevsky L. V., Sokolev S., and Falloon T. J. 2002b. Melt inclusions in olivine phenocrysts: Using diffusive re-equilibration to determine the cooling history of a crystal, with implications for the origin of olivine-phyric volcanic rocks. *Journal of Petrology* 43:1651–1671.

Delano J. and Arculus R. 1980. Nakhla: Oxidation state and other constraints (abstract). 11th Lunar and Planetary Science Conference. pp. 219–221.

Donaldson C. H. 1975. Calculated diffusion coefficients and the growth rate of olivine in a basalt magma. *Lithos* 8:163–174.

Fagan T. J., Scott E. R. D., Keil K., Cooney T. F., and Sharma S. K. 2000. Formation of feldspathic and metallic melts by shock in enstatite chondrite Reckling Peak A80259. *Meteoritics & Planetary Science* 35:319–329.

Fedele L., Bodnar R. J., DeVivo B., and Tracy R. 2003. Melt inclusion geochemistry and computer modeling of trachyte petrogenesis at Ponza, Italy. *Chemical Geology* 194:81–104.

Frezzotti M. L. 2001. Silicate-melt inclusions in magmatic rocks: Applications to petrology. *Lithos* 55:273–299.

Friedman Lentz R. C., Taylor G. J., and Treiman A. H. 1999. Formation of a martian pyroxenite: A comparative study of the nakhlite meteorites and Theo's Flow. *Meteoritics & Planetary Science* 34:919–932.

Gaetani G. A. and Watson E. B. 2000. Open system behavior of olivine-hosted melt inclusions. *Earth and Planetary Science Letters* 183:27–41.

Ghiorso M. S. and Sack R. O. 1991. Fe-Ti oxide geothermometry: Thermodynamic formulation and the estimation of intensive variables in silicic magmas. *Contributions to Mineralogy and Petrology* 108:485–510.

Ghiorso M. S. and Sack R. O. 1995. Chemical mass transfer in magmatic processes, IV. A revised and internally consistent thermodynamic model for the interpolation and extrapolation of liquid-solid equilibria in magmatic systems at elevated temperatures and pressures. *Contributions to Mineralogy and Petrology* 119:197–212.

Hale V. P., McSween H. Y. Jr., and McKay G. A. 1999. Re-evaluation of intercumulus liquid composition and oxidation state for the Shergotty meteorite. *Geochimica et Cosmochimica Acta* 63: 1459–1470.

Harvey R. P. and McSween H. Y. Jr. 1992a. The parent magma of the nakhlite meteorites: Clues from melt inclusions. *Earth and Planetary Science Letters* 111:467–482.

Harvey R. P. and McSween H. Y. Jr. 1992b. The petrogenesis of the nakhlites: Evidence from cumlate mineral zoning. *Geochimica et Cosmochimica Acta* 56:1655–1663.

Johnson M. C., Rutherford M. J., and Hess P. C. 1991. Chassigny petrogenesis: Melt compositions, intensive parameters, and water contents of Martian (?) magmas. *Geochimica et Cosmochimica Acta* 55:349–366.

Kaneda K., McKay G. A., and Le L. 1998. Synthetic and natural pyroxenes: A close match at last (abstract). 29th Lunar and Planetary Science Conference (abstract #1620). CD-ROM.

Longhi J. 1991. Comparative liquidus equilibria of hypersthene-normative basalts at low pressure. *American Mineralogist* 76: 785–800.

Longhi J. and Pan V. 1988. The parent magmas of the SNC meteorites (abstract). 19th Lunar and Planetary Science Conference. pp. 451–464.

Lowenstern J. B. 1995. Application of silicate-melt inclusions to the study of magmatic volatiles. In *Magmas, fluids, and ore deposition*, edited by Thompson J. F. H. Toronto: Mineralogical Association of Canada. pp. 71–98.

Lu F., Anderson A. T. Jr., and Davis A. M. 1995. Diffusional gradients at the crystal/melt interface and their effect on the composition of melt inclusions. *Journal of Geology* 103:591–597.

McSween H. Y. Jr. 1994. What we have learned about Mars from SNC meteorites? *Meteoritics* 29:757–779.

McSween H. Y. Jr. and Harvey R. P. 1993. Outgassed water on Mars: Constraints from melt inclusions in SNC meteorites. *Science* 259:1890–1892.

McSween H. Y. Jr. and Treiman A. H. 1998. Martian meteorites. In *Planetary materials*, edited by Papike J. J. Washington, D. C.: Mineralogical Society of America. pp. 1–53.

Mikouchi T., Koizumu E., Monkawa A., Ueda Y., and Miyamoto M. 2003. Mineralogy and petrology of Yamato-000593: Comparison with other Martian nakhlite meteorites. *Antarctic Meteorite Research* 16:34–57.

Newman S., Epstein S., and Stolper E. 1988. Water, carbon dioxide, and hydrogen isotopes in glasses from the ca. 1340 eruption of Mono Craters, CA: Constraints on degassing phenomena and initial volatile content. *Journal of Volcanology and Geothermal Research* 35:75–96.

Nielsen R. L., Michael P. J., and Sours-Page R. 1998. Chemical and physical indicators of compromised melt inclusions. *Geochimica et Cosmochimica Acta* 62:831–838.

Qin Z., Lu F., and Anderson A. T. Jr. 1992. Diffusive reequilibration of melt and fluid inclusions. *American Mineralogist* 77:565–576.

Reid A. M. and Bunch T. E. 1975. The nakhlites, part II: Where, when, and how. *Meteoritics* 10:317–324.

Roedder E. 1979. Origin and significance of magmatic inclusions. *Bulletin of Mineralogy* 102:487–510.

Sautter V., Barrat J. A., Jambon A., Lorand J. P., Gillet P., Javoy M., Joron J. L., and Lesourd M. 2002. A new Martian meteorite from Morocco: The nakhlite Northwest Africa 817. *Earth and Planetary Science Letters* 195:223–238.

Sisson T. W. and Layne G. D. 1993. H_2O in basalt and basaltic andesite glass inclusions from four subduction-related volcanoes. *Earth and Planetary Science Letters* 117:619–635.

Slater V. P., Thompson C. K., Nettles J., Milam K., Stockstill K. R., Cahill J. T., Anand M. and Taylor L. A. 2003. An evaluation of the igneous crystallization programs—MELTS, MAGPOX, and COMAGMAT Part II: Importance of magmatic fO_2 (abstract #1896). 34th Lunar and Planetary Science Conference. CD-ROM.

Sobolev A. V. 1996. Melt inclusions in minerals as a source of principal petrologic information. *Petrologiya* 4:228–239.

Sobolev A. V., Kamenetskiy V. S., Metrich N., Clocchiatti R., Kononkova N. N., Devirts A. L., and Ustinov V. I. 1990. Volatile regime and crystallization conditions in Etna hawaiite lavas. *Geokhimiya* 9:1277–1290.

Sobolev A. V. and Slutskiy A. B. 1984. Composition and crystallization conditions of the initial melt of the Siberian meimechites in relation to the general problem of ultrabasic magmas. *Soviet Geology & Geophysics* 25:97–110.

Szymanski A., El Goresy A., Brenker F. E., and Palme H. 2003. Application of the Fe-, Ti-thermometer/Oxybarometer to Nakhla and Y-000593 (abstract). Symposium on Evolution of Solar System Materials: A New Perspective From Antarctic Meteorites. pp. 132–133.

Thomas J. B. and Bodnar R. J. 2002. A technique for mounting and polishing melt inclusions in small (<1 mm) crystals. *American Mineralogist* 87:1505–1508.

Thomas J. B., Bodnar R. J., Shimizu N., and Chesner C. 2002. The boundary layer problem and the reliability of melt inclusions as petrogenetic monitors: Evidence from melt inclusions in zircon, allanite, plagioclase and quartz. Proceedings, Workshop-Short Course on Volcanic Systems; Geochemical and Geophysical Monitoring. Melt Inclusions: Methods, Applications and Problems, edited by DeVivo B. and Bodnar R. J. Napoli: De Frede Editore. pp. 205–209.

Treiman A. H. 1985. Amphibole and hercynite spinel in Shergotty and Zagami: Magmatic water, depth of crystallization, and metasomatism. *Meteoritics* 20:229–243.

Treiman A. H. 1986. The parental magma of the Nakhla achondrite: Ultrabasic volcanism on the shergottite parent body. *Geochimica et Cosmochimica Acta* 50:1061–1070.

Treiman A. H. 1990. Complex petrogenesis of the Nakhla (SNC) meteorite: Evidence from petrography and mineral chemistry (abstract). 20th Lunar and Planetary Science Conference. pp. 273–280.

Treiman A. H. 1993. The parent magma of the Nakhla (SNC) meteorite, inferred from magmatic inclusions. *Geochimica et Cosmochimica Acta* 57:4753–4767.

Treiman A. H. 2003. The Nakhla martian meteorite is a cumulate igneous rock. Comment on "Glass-bearing inclusions in Nakhla (SNC meteorite) augite: Heterogeneously trapped phases," 2001, by Varela M. E., Kurat G., and Clocchiatti R. *Mineralogy and Petrology* 76:271–277.

Treiman A. H., Gleason J. D., and Bogard D. D. 2000. The SNC meteorites are from Mars. *Planetary and Space Science* 48: 1213–1230.

Treiman A. H. and Goodrich C. A. 2001. A parent magma for the Nakhla martian meteorite: Reconciliation of estimates from 1-bar experiments, magmatic inclusions in olivine, and magmatic inclusions in augite (abstract #1107). 32nd Lunar and Planetary Science Conference. CD-ROM.

Varela M. E., Kurat G., and Clocchiatti R. 2001. Glass-bearing inclusions in Nakhla (SNC meteorite) augite: Heterogeneously trapped phases. *Mineralogy and Petrology* 71:155–172.

Wadhwa M. and Crozaz G. 1995. Trace and minor elements in minerals of nakhlites and Chassigny: Clues to their petrogenesis. *Geochimica et Cosmochimica Acta* 59:3629–3645.

Wallace P. J., Anderson A. T. Jr., and Davis A. M. 1999. Gradients in H_2O, CO_2, and exsolved gas in a large-volume silicic magma system: Interpreting the record preserved in melt inclusions from the Bishop Tuff. *Journal of Geophysical Research* 104:20,097–20,122.